



30 **Abstract:** An enhanced formation of brown carbon (BrC) with a non-negligible warming effect
31 at the tropopause has recently been found. However, its formation mechanism is unclear. Here
32 we report a BrC formation process that happens during air mass upward transport by
33 conducting simultaneously a 4-hour time resolution of measurement on atmospheric BrC at the
34 mountain foot (MF, 400m a.s.l.) and mountainside (MS, 1120m a.s.l.) of Mt. Hua, China in
35 2016 summer. Our results showed that the daytime light-absorption (Abs_{365nm}) of BrC at MS is
36 approximately 60% lower than that at MF due to a dilution effect caused by the planetary
37 boundary layer expansion, but the daytime light-absorption of BrC relative to black carbon at
38 MS is about 30% higher than that at MF, suggesting a significant formation of secondary BrC
39 in the lifting process of air mass from MF to MS. Such a secondary formation accounted
40 for >50% of BrC at MS but only 27% of BrC at MF. Moreover, N:C elemental ratio of the
41 daytime BrC was 15% higher at MS than that at MF, mainly due to an aerosol aqueous phase
42 formation of water-soluble organic nitrogen (WSON) compounds. Stable nitrogen isotope
43 composition further indicated that such light-absorbing WSON compounds were produced
44 from the aerosol aqueous-phase reaction of carbonyls with NH_4^+ . Our work for the first time
45 revealed that ammonia-induced aerosol aqueous reactions can significantly promote BrC
46 formation during the air mass lifting process, which is probably responsible for an enhanced
47 light absorption of BrC in the upper troposphere.

48 **Keywords:** Brown carbon; Ammonia and carbonyls; Nitrogen-containing organic compounds;
49 Air mass upward transport; Aerosol aqueous-phase reaction.

50



51 **1. Introduction**

52 Light-absorbing organic aerosols, known as brown carbon (BrC), can efficiently absorb
53 solar radiation in the visible to near ultraviolet (UV) wavelength range (Laskin et al., 2015; Liu
54 et al., 2020a; Chakrabarty et al., 2023a) which is corresponding to 27~70% of black carbon
55 (BC) light-absorption in the lower troposphere (Saleh et al., 2015; Lin et al., 2014; Lin et al.,
56 2015) suggesting that BrC can perturb substantially the planetary radiation budget (Qian et al.,
57 2015; Lin et al., 2014; Liu et al., 2015). By absorbing solar radiation at short wavelengths, BrC
58 can strongly alter local gas-phase photochemistry and atmospheric oxidation through
59 decreasing the photolysis rates of OH radicals, NO₂ and O₃, leading to a reduction in
60 atmospheric oxidant concentration by up to ~30% (Hammer et al., 2016; Gligorovski et al.,
61 2015; Jo et al., 2016). BrC in the atmosphere also acts as photosensitizers and produces active
62 intermediates, and thus can promote sulfate formation (Liu et al., 2020b). In addition, BrC
63 comprises numerous organic species and can induce adverse human health effects, because
64 some of chromophores are toxic (Huang et al., 2018; Hsu et al., 2014; Yan et al., 2018).

65 Atmospheric BrC has both primary and secondary sources. Biomass burning is believed to
66 be the major source of primary BrC (Chakrabarty et al., 2023b), while emissions from fossil
67 fuel combustion is also an important source of primary BrC in the urban atmosphere (Yan et al.,
68 2017; Corbin et al., 2019), which accounts for even more than 40% of the total BrC in heating
69 season (Li et al., 2023). In the past decades numerous studies reported that BrC can also be
70 secondarily generated in the atmosphere, such as photooxidation of aromatics under high NO_x
71 conditions (Lin et al., 2015; Liu et al., 2021), NH₄⁺-initiated reactions with atmospherically
72 relevant carbonyls (Li et al., 2021b; Kampf et al., 2012; Laskin et al., 2014; Li et al., 2019b)



73 and $\cdot\text{OH}/\text{NO}_3\cdot$ radical oxidations of various VOCs (Sumlin et al., 2017; Gelencser et al., 2003;
74 Lu et al., 2011). BrC is chemically active, which may undergo photobleaching (Schnitzler et al.,
75 2022; Gilardoni et al., 2016), posing significant challenges for characterizing BrC molecular
76 composition and its links to optical properties.

77 Recently a aircraft measurement conducted over the continental United States observed an
78 enhanced short-wavelength optical absorption of BrC relative to BC at altitudes between 5 and
79 12 km (Zhang et al., 2017), indicating that secondary formation is one of crucial sources for
80 these high-altitude BrC. Numerical model studies reported that global radiative forcing caused
81 by BrC ranges from $0.1\text{-}0.6\text{ Wm}^{-2}$, suggesting a non-negligible impact of BrC on the global
82 climate change. Studies found that such climate effects are highly sensitive to BrC and the
83 sensitivity rapidly increases along with an increase in altitude (Zhang et al., 2017; Nazarenko et
84 al., 2017; Hodnebrog et al., 2014). These abundant BrC at the tropopause would bring about
85 prominent impacts on radiative forcing, which is even twice of that induced by low-altitude
86 BrC (Zhang et al., 2017). Due to the limited number of field observations, however, the vertical
87 distribution and formation mechanism of tropospheric BrC are still unclear especially those in
88 the upper troposphere, where the direct radiative forcing of BrC is much stronger than that in
89 the ground surface atmosphere.

90 To elucidate the formation mechanism of BrC in the troposphere, synchronous
91 observations on atmospheric BrC were conducted on the mountainside and the mountain foot
92 of Mt. Hua, which is located closely to Guanzhong Basin, one of the areas with heaviest $\text{PM}_{2.5}$
93 pollution in China owing to intensive activities of fossil fuel combustion and the unfavorable
94 topography (Wang et al., 2022b; Wu et al., 2020; Wang et al., 2011; Wang et al., 2016). Our



95 previous study has shown that inorganic aerosol chemistry in the atmosphere over Mt. Hua is
96 dominated by the air mass transport from the Guanzhong Basin ground surface, in which
97 $(\text{NH}_4)_2\text{SO}_4$ is continuously produced during the air mass lifting process along with a decrease
98 in aerosol acidity (Wu et al., 2022). Here, we investigated the formation mechanism of
99 secondary BrC during the lifting process of air mass from the Guanzhong Basin to the
100 mountainous atmosphere of Mt. Hua. We firstly discussed the differences in vertical
101 distribution and optical absorption of water-soluble BrC between the ground surface and the
102 mountainous atmosphere, then explored their formation mechanism in the upper troposphere.
103 To the best of our knowledge, we for the first time found that ammonia-induced aerosol
104 aqueous phase reaction with carbonyls is the dominant formation pathway of BrC in the air
105 mass lifting process, which is responsible for the high ratio of BrC to BC in the top
106 troposphere.

107 **2. Materials and Methods**

108 **2.1 Sample Collection**

109 $\text{PM}_{2.5}$ samples with a 4-hour interval were synchronously collected at two locations of Mt.
110 Hua from 27 August to 17 September 2016. One sampling site locates at the mountain foot (MF,
111 $34^\circ 32' \text{N}$, $110^\circ 5' \text{E}$) and another one is situated on the mountainside (MS; $34^\circ 29' \text{N}$, $110^\circ 3' \text{E}$) with
112 little anthropogenic activities due to its steep terrain in the mountain region. The horizontal
113 distance between the two sites is ~ 8 km and the vertical distance is about 1 km (Figure S1). More
114 descriptions on the two sites have been documented by our previous study along with the details
115 on the sampling instrument setup (Wu et al., 2022). Hourly concentrations of $\text{PM}_{2.5}$, NO_2 and O_3
116 at MS site were monitored by E-BAM (Met One Instruments, USA) and NO_x and O_3 Analyzer



117 (Thermo, Model 42i, USA; Thermo, Model 49i, USA), respectively. Meteorological parameters
118 of both sampling sites were downloaded from the Shaanxi Meteorological Bureau website
119 (<http://sn.cma.gov.cn/>).

120 **2.2 Chemical Analysis**

121 A DRI model 2001 thermal–optical carbon analyzer was used to measure the organic
122 carbon (OC) and element carbon (EC) of PM_{2.5} filter samples. Water-soluble organic carbon
123 (WSOC) and water-soluble total nitrogen (WSTN) of PM_{2.5} were extracted using Milli-Q pure
124 water (18.2 MΩ) and determined using a total organic carbon (TOC) analyzer (Model TOC-L
125 CPH, Shimadzu, Japan). Water-soluble organic nitrogen (WSON) is calculated by deducting
126 the water-soluble inorganic nitrogen (WSIN) from WSTN (i.e., WSON=WSTN-WSIN).
127 Molecular compositions (e.g., nitrophenols, PAHs and other organic tracers) in the PM_{2.5} filter
128 samples were quantified by a gas chromatography (HP 7890A, Agilent Co., USA) coupled with
129 mass spectroscopy detector (GC/MS) (HP 5975, Agilent Co., USA) after the sample extraction
130 and derivatization. Th details of the extraction and derivatization can be found elsewhere (Li et
131 al., 2023; Li et al., 2020; Wang et al., 2006). Briefly, one-fourth of the filter sample was
132 extracted with a mixture of methanol and dichloromethane (2:1, v/v). Then the extracts were
133 derivatized with N,O-bis-(trimethylsilyl) trifluoroacetamide (BSTFA).

134 Additionally, a high-resolution time-of-flight aerosol mass spectrometer (Aerodyne
135 Research Inc., Billerica, MA, USA) was employed to determine the chemical compositions of
136 water-soluble organic matter (WSOM) in PM_{2.5}, of which the method is similar to the report by
137 Daellenbach et al. (2016). The offline analytical procedure has been reported previously, here
138 we only give a brief description (Ge et al., 2017; Sun et al., 2011). One-eighth of the PM_{2.5}



139 filter samples was extracted with pure water. Then, the water-extracts were atomized using
140 argon as carrier gas, dried by a diffusion drier, and ultimately quantified by the aerosol mass
141 spectrometer. Purified water was also treated in the same manner prior to each sample running,
142 which was deemed as an analytical blank. As we mainly focused on the WSOM chemical
143 composition, a deep post-processing was conducted for the V-mode data in this study using the
144 Igor-based Aerosol Mass Spectrometer Analysis Toolkit. Element ratios of WSOM including
145 oxygen-to-carbon (O/C), hydrogen-to-carbon (H/C), nitrogen-to-carbon (N/C), and organic
146 mass-to-organic carbon (OM/OC) ratios were determined according to the Improved Aiken (I-
147 A) method (Canagaratna et al., 2015). The mass load of WSOM in ambient air can be
148 accurately estimated using Eq.1, since the chemical species concentration in atomized aerosols
149 depends on the flow rate of the carrier gas and extract concentration.

$$\text{WSOM} = \text{WSOC} \times \text{OM/OC}_{\text{WSOM}} \quad \text{Eq. 1}$$

150 Where WSOM is water-soluble organic matter (WSOM) in the atmosphere ($\mu\text{g m}^{-3}$),
151 WSOC is water-soluble organic carbon (WSOC, μgCm^{-3}) in the atmosphere and measured by
152 the TOC analyzer, and $\text{OM/OC}_{\text{WSOM}}$ is the mass ratio of WSOM and OC determined by the
153 aerosol mass spectrometer.

154 **2.3 Optical Absorption of BrC**

155 Measurement of UV-vis absorption spectra of water-soluble BrC in $\text{PM}_{2.5}$ was performed
156 using a liquid waveguide capillary UV-vis spectrometer with a long effective path length (1
157 m). The extracted solution of BrC were prepared by a similar treatment to WSOC (Text S1), of
158 which absorption spectra were converted into the absorption coefficient at a given wavelength λ
159 (abs_{λ} , M/m, eq S1). The mass absorption efficiency (MAE_{λ} , m^2/gC) corresponding to water-



160 soluble BrC at a given wavelength λ can be calculated as follows:

$$\text{MAE}_\lambda = \frac{\text{abs}_\lambda}{M} \quad \text{Eq. 2}$$

161 Where M ($\mu\text{gC}/\text{m}^3$) is the mass concentration for water-soluble organic carbon (WSOC).

162 Absorption Ångström exponent (AAE) indicates the spectral dependence of a species, which
163 was quantified by a linear regression of $\log(\text{abs}_\lambda)$ versus $\log(\lambda)$ over a wavelength rang of 300-
164 500 nm (Wu et al., 2020).

165 **2.4 Random forest analysis for WSON**

166 Random forest (RF), as a powerful tool, has been used widely in the regression and prediction
167 problems upon atmospheric pollutions, even the data have complex nonlinear relationships and
168 interactions (Hu et al., 2017; Vu et al., 2019). To reveal the key factors that may affect the WSON
169 formation during the air mass lifting process, the RF analysis was applied for the daytime samples
170 at MF and MS sites, respectively. And the potential factors, including pH, ALWC, T, RH, NH_4^+ ,
171 $\text{NH}_3(\text{aq})$, NO_2 , nitrophenols, O_3 and organic matter (OM), herein were regarded as the predictors
172 for WSON. In the RF model design, about 70% of these original data were randomly divided
173 into the training dataset to construct the RF model, and the rest was deemed as the testing data
174 for testing the model performance as testing datasets. To evaluate the performance of the RF
175 model to reconstruct the WSON, three established and robust error measurement metrics were
176 employed here, including correlation coefficients (R^2), mean square error (MSE) or root-mean-
177 square error (RMSE) and mean absolute error (MAE). As shown in Table S1, the predicted data
178 for the testing dataset has strong correlativity with observed ones, with small values for those
179 error metrics; These results indicated a satisfactory performance of the RF model for
180 investigating contributions of these factors to WSON formation.



181 **3. Results and Discussion**

182 **3.1 Enhanced Light Absorption of BrC in the Mountainous Atmosphere**

183 Figure 1 shows the temporal variations in light absorption (abs_{365nm}) and concentrations of
184 fine particulate WSOC simultaneously observed at the mountain foot (MF) and mountainside
185 (MS) sites. Light absorption of BrC at the two sites markedly increased with a decrease in light
186 wavelengths. The averaged abs_{365nm} of BrC was $2.1 \pm 1.4 M m^{-1}$ at MS, approximately
187 corresponding to 40% of that ($5.1 \pm 2.4 M m^{-1}$, Table 1) at MF. The light-absorbance level of
188 BrC at the high altitude MS site is in the same range as those reported from Chinese megacities
189 such as Beijing (Cheng et al., 2016) and Xi'an (Wu et al., 2020), indicating a strong light-
190 absorption of BrC in the upper boundary layer over Guanzhong Basin, inland China.
191 Absorption Ångström exponent (AAE) at MS is 5.7 ± 1.3 (Table 1), slightly lower than that at
192 the ground MF site (6.0 ± 0.5). Such a difference in AAE ($p < 0.05$) is most likely related to the
193 difference in chemical composition of the chromophores between the two sites with different
194 altitudes. As shown in Figure 1, the water-soluble BrC (i.e., abs_{365nm}) closely followed the
195 variation patterns of WSOC ($R^2 > 0.70$, Figure S2) at both sites, indicating that BrC is an
196 important part of WSOC. The averaged mass absorption efficiency (MAE) at MS (MAE_{365nm} ,
197 $0.67 \pm 0.2 m^2 g^{-1}$) was almost equal to that at MF ($0.69 \pm 0.2 m^2 g^{-1}$) but 30-40% higher than those
198 observed in Chinese megacities such as Beijing (Du et al., 2014) and Nanjing (Chen et al.,
199 2018) ($\sim 0.5 m^2 g^{-1}$, in summertime), further demonstrating a strong light-absorption nature of
200 BrC in the upper boundary layer of Guanzhong Basin, inland China.

201 Figure 2 shows the diurnal variations of abs_{365nm} and MAE_{365nm} at both sites during the
202 campaign. At MF site a morning peak of abs_{365nm} driven by enhanced traffic emissions



203 occurred at 8:00~12:00 (local time, thereafter), and then gradually decreased and reached a
204 minimum at 12:00~16:00 with the lowest MAE at 365 nm wavelength ($MAE_{365\text{ nm}}, 0.57\pm 0.14$
205 $\text{m}^2\text{ g}^{-1}$ (Figures 2a and 2b). Such a ground surface decrease in light absorption of BrC at early
206 afternoon can be attributed to the daytime boundary layer growth and photobleaching. This can
207 be verified by the oxidation state of carbon (OSc) measured by the aerosol mass spectrometer,
208 of which higher value is indicative of a deeper degree of atmospheric oxidation (Li et al.,
209 2019a). As seen in Figure 3a, $abs_{365\text{ nm}}$ negatively correlated with OSc, which is consistent with
210 those reported by previous laboratory experiments (Lee et al., 2014; Zhao et al., 2015; Sumlin
211 et al., 2017) and suggests that atmospheric aging can significantly diminish the light-absorption
212 of BrC. On the contrary, $abs_{365\text{ nm}}$ at MS site remarkably enhanced with the boundary layer
213 growth and peaked at 12:00~16:00 (Figure 2a), despite the fact that the aerosol was further
214 oxidized during the upward transport as indicated by the OSc values, which are higher at MS
215 than at MF (Figure 3b). Moreover, a moderate-increased $MAE_{365\text{ nm}}$ was also observed in this
216 process (Figure 2b). As shown in Table 1, the light absorption of BrC at 365 nm relative to BC
217 at 550 nm ($abs_{365\text{ nm}}\text{-BrC}/abs_{550\text{ nm}}\text{-BC}$) during the daytime at MS was 0.28 ± 0.08 , which is
218 approximately 30% higher than that (0.22 ± 0.08 , Table 1) at MF. Our previous study at Mt. Hua
219 found that changes in sources of primary organic aerosols in the air mass transported from MF
220 to MS were insignificant (Wu et al., 2022), indicating that there was no additional emission of
221 BrC during the air mass upward transport. Thus, the enhanced light-absorption of BrC relative
222 to BC at MS is solely ascribed to a secondary formation of absorbing BrC (Figure 2c); and
223 these secondary BrC were highly light-absorbing despite more aged atmosphere aloft, as
224 verified by a strongly positive correlation between $MAE_{365\text{ nm}}$ and OSc values at MS site



225 (Figure S3).

226 To further elucidate the above hypothesis, a PMF analysis (Text S2) was applied for the
227 source apportionment of the daytime $\text{abs}_{365\text{ nm}}$ at both sites. As seen in Figure S4, four types of
228 BrC sources were identified. In brief, fossil fuel combustion and biomass burning influenced by
229 local-related emissions were primary sources for the surface BrC, consistent with observations
230 in other cities (Li et al., 2023; Wu et al., 2020; Wang et al., 2022a). However, BrC at MS site
231 was produced dominantly from secondary formation, of which the contribution to the total BrC
232 is 53% and about twice of that at MF (Figure 2d,) further corroborating a substantial formation
233 of BrC with relatively stronger light-absorptivity during the air mass lifting process. These
234 secondarily formed BrC chromophores engender a more light-absorption of high-altitude BrC
235 compared with that of BC (or EC, Figure 2c), coincident with the in-situ aircraft measurements
236 over the continental US and Beibu Gulf of China (Zhang et al., 2017; Yang et al., 2023),
237 indicating that such a vertical profile of BrC is globally prevalent in the upper troposphere.

238 **3.2 Secondary Formation of BrC in the Air Mass Lifting Process**

239 Figure 4a illustrates the diurnal cycles of N:C ratio of the water-soluble organic matter in
240 $\text{PM}_{2.5}$ measured by the high-resolution time-of-flight aerosol mass spectrometer. At the MF site
241 N:C ratio did not vary much with time and was even leveling off in the daytime, which
242 indicates that the compositions of light-absorbing chromophores are similar throughout the day.
243 Nonetheless, the diurnal pattern of N:C ratio at MS was analogous to that of $\text{abs}_{365\text{ nm}}$ and
244 $\text{MAE}_{365\text{ nm}}$ with a daily peak at 12:00~16:00 and a moderate positive correlation was also
245 observed between N:C ratio and $\text{abs}_{365\text{ nm}}$ ($R^2=0.38$, $P<0.01$), suggesting that nitrogen-
246 containing organic compounds (NOCs) have considerable contributions to the BrC light-



247 absorption in the upper troposphere. Such a results is consistent with the laboratory simulation,
248 in which NOCs have been reported to contribute up to 60% of the absorbance of secondary BrC
249 over a wavelength rang of 300–400 nm (Lin et al., 2015). Moreover, the daytime N:C ratios
250 were 20% higher at MS (0.066 ± 0.014) than those at MF (Figure 4a), indicating that additional
251 NOCs were produced in the air mas lifting process. In fact, numerous N-containing organic
252 fragments including C_xH_yN and $C_xH_yO_zN$ at the MS site were detected by the aerosol mass
253 spectrometer, which accounted for ~13% of the total water-soluble OM and was 20% higher
254 than that at the MF site (Figure S5), clearly suggesting an enhanced formation of WSON during
255 the air mass transport from the lower mountain foot site to the upper mountainside site. Since
256 WSON at MS strongly was positively correlated with light absorption of BrC at $\lambda=365\text{nm}$
257 (Figure S6), the enhancement in BrC light-absorption at MS can largely be attributed to
258 secondary formation of NOCs during the air mass transport from the ground surface to the
259 upper boundary layer.

260 Light-absorbing NOCs including reduced nitrogen species (e.g., imidazoles and pyrazines)
261 and oxidized ones (e.g., nitroaromatics) can be generated via various types of gas- and particle-
262 phase reactions, such as, NH_3 -mediated carbonyl-to-imine reactions, nitration of aromatic
263 compounds, and heterogeneous reactions of $\cdot\text{OH}$ and $\text{NO}_2\cdot$ radicals with phenolic compounds
264 (Moise et al., 2015; Laskin et al., 2015). The potential pathways and dominating factors for
265 NOCs formation at MS site will be explored in the following sections.

266 **3.3 Gas-Phase Formation of BrC in the Air Mass Lifting Process**

267 Nitroaromatic compounds (NACs) are strong light-absorbing compounds and are
268 ubiquitous in the atmosphere. In this study, a total of six NACs in the $\text{PM}_{2.5}$ samples were



269 detected (Table S2), which exhibited a significant correlation with $\text{abs}_{365 \text{ nm}}$ at both sampling
270 sites (Figure S2c and S2d), indicating an important impact of NACs on the aerosol light-
271 absorption. As seen in Figure 5a, both NACs concentration and NACs/OC ratio decreased
272 gradually at MF, reaching the daily minimum at 12:00-16:00. Such an abatement in NACs was
273 mainly attributed to the boundary layer expansion and an enhanced photooxidation (Figure 3).
274 Furthermore, the daytime NACs at MF well correlated with (BbF+levoglucosan), which are
275 tracers for combustion emissions ($R^2=0.70$), but not correlated with gaseous NO_2 (Figure 5e),
276 suggesting that most of NACs at the ground surface site were directly emitted from combustion
277 sources. As partial NACs at the MF site can be transported aloft by anabatic valley winds, thus
278 a moderate correlation ($R^2=0.49$, Figure 5d) between NACs and (BbF+levoglucosan) was
279 observed at MS site. However, a strong correlation between NO_2 and NACs ($R^2=0.57$, Figure
280 5f) observed at MS suggests a non-negligible formation of secondary NACs under the transport
281 process. Previous studies reported that NACs could be produced via gas-phase or aqueous
282 reactions under higher $\text{NO}_x/\text{NO}_3^-/\cdot\text{OH}$ conditions (Wang and Li, 2021; Li et al., 2021a). But a
283 poor relationship between NACs and ALWC ($R^2=0.34$, $P>0.05$), indicating that the gas-phase
284 reaction is a dominant formation pathway for nitrophenols aloft. Moreover, the aerosol pH
285 simulated by our previous study was higher at MF (3.4 ± 2.2) than that at MS (2.9 ± 2.0) (Wu et
286 al., 2022). Such a decreasing acidity condition can promote the protonation of NACs and thus
287 enhance their light-absorption at visible wavelengths (Liu et al., 2023b).

288 The preceding discussion provided explicit evidence that partial NACs could be formed by
289 gas-phase reactions, but they only accounted for a very small fraction of OC (Figure 5a-b),
290 suggesting that gas-phase formation is probably not the major formation pathway of secondary



291 NOCs during the air mass vertical transport. Further evidence for this hypothesis was provided
292 by a random forest (RF) analysis that was used for quantifying the contributions of these
293 influencing factors (aerosol liquid water content (ALWC), pH, T, NO₂, NH₄⁺, etc.) to WSON at
294 both sampling sites (Figure 4b and Figure S7). As revealed by RF model results, nitrophenols
295 and gaseous NO₂ factors together explained up to 35% of the daytime WSON at MF site
296 (Figure S7) but only ~15% of that aloft (Figure 4b), confirming a less importance of the gas-
297 phase reactions for the light-absorbing NOCs formation in the upper troposphere.

298 **3.4 Aerosol Aqueous Formation of BrC in the Air Mass Lifting Process**

299 As shown in Figure 4b, RF analysis showed that the variation in concentration of WSON
300 in PM_{2.5} at MS was largely affected by NH₄⁺ (23.0%) and ALWC (17.3%). Given a relatively
301 strong correlation between WSON and NH₄⁺ (R²=0.70, Figure 4c), we proposed that aqueous
302 phase reactions induced by ammonium is the major formation pathway for water-soluble NOCs
303 at MS. For further demonstrating such a hypothesis, we analyzed nitrogen isotope composition
304 (δ¹⁵N-NH₄⁺) of ammonium in the PM_{2.5} samples at both sites, of which the analytical details
305 has been described in our previous study (Wu et al., 2022). As seen in Figure 4d, WSON
306 showed a strong negative correlation with δ¹⁵N-NH₄⁺, because a lighter isotope reacts at a
307 faster rate due to its higher zero-point energy, which can result in the products enriched in
308 lighter ¹⁴N and depleted in heavier ¹⁵N during the NH₃ neutralization process. In contrast,
309 WSON at MF presented a similar correlation with NH₄⁺ as that at MS but did not correlate with
310 δ¹⁵N-NH₄⁺ (Figures S8a and b).

311 Previous studies have demonstrated the importance of NH₄⁺/NH₃ in the formation of light-
312 absorbing imidazoles and N-heterocycles from the carbonyls (e.g., glyoxal (Gly) and



313 methylglyoxal (mGly) generated from oxidation of VOCs (Li et al., 2021b; Moise et al., 2015;
314 Kampf et al., 2012; Liu et al., 2023a). Figure S9 depicts a simple reaction pathway for above
315 aqueous reactions, in which the chromophore products contain less amounts of O and H atoms.
316 Such a phenomenon was found for the daytime NOCs at MS. As shown in Figure S10, the H/N
317 and O/N ratios of BrC in PM_{2.5} at MS exhibited a strongly negative correlation with N/C ratio,
318 respectively ($R^2=0.92$ for H/N and $R^2=0.84$ for O/N). Considering the fact that Gly and mGly
319 are abundant at the daytime atmosphere of Mt. Hua (Qi et al., 2023), the aqueous reactions of
320 dicarbonyls with $\text{NH}_4^+/\text{NH}_3$ are probably the major pathway to yield NOCs during the vertical
321 transport.

322 Above aqueous reactions could also occur at MF site as depicted in Figure S8, but it was
323 insignificant compared to that at MS site, attributing the disparity in chemical compositions.
324 Our previous study found that the ground surface MF aerosols were more acidic (pH=2.9) and
325 dominated by NH_4HSO_4 , while the upper boundary layer MS aerosols were less acidic
326 (pH=3.4) and dominated by abundant $(\text{NH}_4)_2\text{SO}_4$. Such differences in aerosol acidity and
327 chemical compositions between two sites can favor the formation of NOCs at the MS site, as
328 evident from a recent experimental observation by Li et al. (2021b), who found that NOCs
329 yield on the $(\text{NH}_4)_2\text{SO}_4$ seeds exposing to Gly or mGly vapor was relatively higher than that on
330 NH_4HSO_4 seeds. Also, they found that mGly has a larger uptake coefficient on $(\text{NH}_4)_2\text{SO}_4$
331 particles with a relatively higher NOCs yield compared to Gly, because mGly has a stronger
332 interfacial attraction and thus has a more efficient nucleophilic addition involving the
333 carbenium ions (Li et al., 2021b). Our previous study showed that the summertime atmosphere
334 of Mt. Hua is dominated by biogenic VOCs and the concentration of fine particulate mGly is



335 about five times that of Gly (Meng et al., 2014). Such a predominance of mGly over Gly and a
336 less acidic aerosol aqueous aerosol phase at the MF site are favorable for light-absorbing NOCs
337 formation on $(\text{NH}_4)_2\text{SO}_4$ particles, which can mainly be responsible for the enhanced light
338 absorption of BrC at the mountainous site with the ratio of light absorption of BrC to BC higher
339 in the upper boundary layer than that in the ground surface.

340 **4. Conclusion and atmospheric implications**

341 Our work provides an evolution profile of BrC during air mass vertical transport, and
342 highlights a rapid formation of BrC in this process, which can be responsible for the
343 enhancement of BrC relative to BC in the upper troposphere. As revealed by aircraft
344 observation over the continental US (Zhang et al., 2017), the high-altitude BrC have longer
345 lifetime, and can disperse rapidly into a large area, exerting significant influence on regional
346 climate. The heating effect of BrC is even comparable to BC in the upper tropical troposphere
347 (Jo et al., 2016). In this work, we revealed a vital role of aqueous-phase reactions for the
348 secondary formation of BrC in the air mass lifting process, specifically the $\text{NH}_4^+/\text{NH}_3$ -induced
349 reactions (e.g., Maillard reaction) that can form NOCs with stronger light-absorptivity. As
350 ammonia and carbonyls such as glyoxal and methylglyoxal are ubiquitous in the troposphere,
351 thus our work suggests that the above formation mechanism on the light-absorbing NOC
352 aerosols could extensively occur in the troposphere.

353 In the past decade, the haze pollution in China has changed from previous sulfate-
354 dominated environment (SD) to the current nitrate-dominated environment (ND) due to the
355 effective sulfur emission control, which would significantly enhance the aerosol ALWC since
356 nitrate is more hygroscopic than sulfate at a given RH and aerosol loading. While, as indicated



357 by our previous observational evidences (Lv et al., 2023), high ALWC load induced by
358 abundant nitrate would efficiently promote more WSOC partitioning into the aerosol phase
359 compared with that in SD ones, and thus may increase the BrC yield because WSOC contains
360 numerous BrC precursors. With the increase in relative abundance of nitrate to sulfate, nitrate-
361 enhanced gas-to-particle partitioning of WSOC will become highly efficient in China in the
362 near future, meaning that the BrC formation will be more active hereafter. Additionally, the
363 national VOCs and NH₃ emissions have remained at high levels, and even have shown a slight
364 increasing trend. The abundant NH₃ can not only participates in the formation of BrC but also
365 affects BrC optical properties by regulating the aerosol acidity. To further reveal the impact on
366 the BrC, the NH₃ concentration and MAE_{365 nm} value of water-soluble BrC in different region
367 of China were statistically explored on a national scale (Figure 6a). As depicted in Figure 6, the
368 spatial pattern of MAE_{365 nm} is closely coincident with NH₃ levels with a robust positive
369 correlation ($R^2=0.87$). Such a spatial distribution pattern indicates that NH₃-rich conditions are
370 favorable for formation of BrC with strong light-absorptivity. China is one of the countries with
371 strongest NH₃ emissions in the world due to huge demand for N-fertilizer (Van Damme et al.,
372 2018), and thus atmospheric NH₃ in China is much higher than that in Europe and the United
373 States. This is probably one of the factors causing the higher concentrations of BrC with
374 stronger light-absorptivity in China compared with developed countries (Figure 6b). Therefore,
375 NH₃ emission control in China is indispensable for further alleviating haze and BrC pollutions
376 in the country.

377 **Data availability.** The data used in this study are freely available at

378 <https://doi.org/10.5281/zenodo.10926469> (Wu, 2024). And Meteorological data and hourly



379 PM_{2.5}, NO₂, O₃ concentrations can be obtained from <https://doi.org/10.5281/zenodo.7413640>
380 (Wu, 2022a).

381 **Author contributions.** G.W. designed research and contributed analytic tools. C.W., C.C. and
382 J.L. collected the samples. C.W., X.L., K.Z. and G.W. conducted the sample analysis. C.W.,
383 S.Z. and G.W. performed the data interpretation. C.W. and G.W. wrote the paper. All authors
384 contributed to the paper with useful scientific discussions.

385 **Competing interests.** The authors declare no competing interest.

386 **Acknowledgements.** This work was financially supported by the National Natural Science
387 Foundation of China (No. 42130704, 42007202) and ECNU Happiness Flower program.

388

389 **References**

- 390 Bosch, C., Andersson, A., Kirillova, E. N., Budhavant, K., Tiwari, S., Praveen, P. S., Russell, L. M., Beres, N. D.,
391 Ramanathan, V., and Gustafsson, O.: Source-diagnostic dual-isotope composition and optical properties of
392 water-soluble organic carbon and elemental carbon in the South Asian outflow intercepted over the Indian
393 Ocean, *J. Geophys. Res.-Atmos.*, 119, 11743-11759, 10.1002/2014jd022127, 2014.
- 394 Canagaratna, M. R., Jimenez, J. L., Kroll, J. H., Chen, Q., Kessler, S. H., Massoli, P., Hildebrandt Ruiz, L., Fortner,
395 E., Williams, L. R., Wilson, K. R., Surratt, J. D., Donahue, N. M., Jayne, J. T., and Worsnop, D. R.: Elemental
396 ratio measurements of organic compounds using aerosol mass spectrometry: characterization, improved
397 calibration, and implications, *Atmos. Chem. Phys.*, 15, 253-272, 10.5194/acp-15-253-2015, 2015.
- 398 Chakrabarty, R. K., Shetty, N. J., Thind, A. S., Beeler, P., Sunlin, B. J., Zhang, C., Liu, P., Idrobo, J. C., Adachi, K.,
399 Wagner, N. L., Schwarz, J. P., Ahern, A., Sedlacek, A. J., Lambe, A., Daube, C., Lyu, M., Liu, C., Herndon, S.,
400 Onasch, T. B., and Mishra, R.: Shortwave absorption by wildfire smoke dominated by dark brown carbon, *Nat.*
401 *Geosci.*, 16, 683-+, 10.1038/s41561-023-01237-9, 2023a.
- 402 Chakrabarty, R. K., Shetty, N. J., Thind, A. S., Beeler, P., Sunlin, B. J., Zhang, C. C., Liu, P., Idrobo, J. C., Adachi,
403 K., Wagner, N. L., Schwarz, J. P., Ahern, A., Sedlacek, A. J., Lambe, A., Daube, C., Lyu, M., Liu, C., Herndon,
404 S., Onasch, T. B., and Mishra, R.: Shortwave absorption by wildfire smoke dominated by dark brown carbon,
405 *Nature Geoscience*, 16, 10.1038/s41561-023-01237-9, 2023b.
- 406 Chen, Y., Ge, X., Chen, H., Xie, X., Chen, Y., Wang, J., Ye, Z., Bao, M., Zhang, Y., and Chen, M.: Seasonal light
407 absorption properties of water-soluble brown carbon in atmospheric fine particles in Nanjing, China, *Atmos.*
408 *Environ.*, 187, 230-240, 10.1016/j.atmosenv.2018.06.002, 2018.
- 409 Cheng, Y., He, K.-b., Du, Z.-y., Engling, G., Liu, J.-m., Ma, Y.-l., Zheng, M., and Weber, R. J.: The characteristics
410 of brown carbon aerosol during winter in Beijing, *Atmos. Environ.*, 127, 355-364,
411 10.1016/j.atmosenv.2015.12.035, 2016.
- 412 Corbin, J. C., Czech, H., Massabo, D., de Mongeot, F. B., Jakobi, G., Liu, F., Lobo, P., Mennucci, C., Mensah, A.
413 A., Orasche, J., Pieber, S. M., Prevot, A. S. H., Stengel, B., Tay, L. L., Zanatta, M., Zimmermann, R., El Haddad,



- 414 I., and Gysel, M.: Infrared-absorbing carbonaceous tar can dominate light absorption by marine-engine exhaust,
415 *npj Clim. Atmos. Sci.*, 2, 10.1038/s41612-019-0069-5, 2019.
- 416 Daellenbach, K. R., Bozzetti, C., Krepelova, A. K., Canonaco, F., Wolf, R., Zotter, P., Fermo, P., Crippa, M., Slowik,
417 J. G., Sosedova, Y., Zhang, Y., Huang, R. J., Poulain, L., Szidat, S., Baltensperger, U., El Haddad, I., and Prevot,
418 A. S. H.: Characterization and source apportionment of organic aerosol using offline aerosol mass spectrometry,
419 *Atmospheric Measurement Techniques*, 9, 23-39, 10.5194/amt-9-23-2016, 2016.
- 420 Du, Z., He, K., Cheng, Y., Duan, F., Ma, Y., Liu, J., Zhang, X., Zheng, M., and Weber, R.: A yearlong study of water-
421 soluble organic carbon in Beijing II: Light absorption properties, *Atmospheric Environment*, 89, 235-241, 2014.
- 422 Ge, X., Li, L., Chen, Y., Chen, H., Wu, D., Wang, J., Xie, X., Ge, S., Ye, Z., Xu, J., and Chen, M.: Aerosol
423 characteristics and sources in Yangzhou, China resolved by offline aerosol mass spectrometry and other
424 techniques, *Environ. Pollut.*, 225, 74-85, 10.1016/j.envpol.2017.03.044, 2017.
- 425 Gelencser, A., Hoffer, A., Kiss, G., Tombacz, E., Kurdi, R., and Bencze, L.: In-situ formation of light-absorbing
426 organic matter in cloud water, *Journal of Atmospheric Chemistry*, 45, 25-33, 10.1023/a:1024060428172, 2003.
- 427 Gilardoni, S., Massoli, P., Paglione, M., Giulianelli, L., Carbone, C., Rinaldi, M., Decesari, S., Sandrini, S., Costabile,
428 F., Gobbi, G. P., Pietrogrande, M. C., Visentin, M., Scotto, F., Fuzzi, S., and Facchini, M. C.: Direct observation
429 of aqueous secondary organic aerosol from biomass-burning emissions, *Proceedings of the National Academy
430 of Sciences of the United States of America*, 113, 10013-10018, 10.1073/pnas.1602212113, 2016.
- 431 Gligorovski, S., Strekowski, R., Barbat, S., and Vione, D.: Environmental Implications of Hydroxyl Radicals (\bullet OH),
432 *Chem. Rev.*, 115, 13051-13092, 10.1021/cr500310b, 2015.
- 433 Hammer, M. S., Martin, R. V., van Donkelaar, A., Buchard, V., Torres, O., Ridley, D. A., and Spurr, R. J. D.:
434 Interpreting the ultraviolet aerosol index observed with the OMI satellite instrument to understand absorption
435 by organic aerosols: implications for atmospheric oxidation and direct radiative effects, *Atmos. Chem. Phys.*,
436 16, 2507-2523, 10.5194/acp-16-2507-2016, 2016.
- 437 Hodnebrog, O., Myhre, G., and Samset, B. H.: How shorter black carbon lifetime alters its climate effect, *Nature
438 Communications*, 5, 10.1038/ncomms6065, 2014.
- 439 Hsu, H.-I., Lin, M.-Y., Chen, Y.-C., Chen, W.-Y., Yoon, C., Chen, M.-R., and Tsai, P.-J.: An Integrated Approach to
440 Assess Exposure and Health-Risk from Polycyclic Aromatic Hydrocarbons (PAHs) in a Fastener
441 Manufacturing Industry, *International Journal of Environmental Research and Public Health*, 11, 9578-9594,
442 10.3390/ijerph110909578, 2014.
- 443 Hu, X., Belle, J. H., Meng, X., Wildani, A., Waller, L. A., Strickland, M. J., and Liu, Y.: Estimating
444 $PM_{2.5}$ Concentrations in the Conterminous United States Using the Random Forest Approach,
445 *Environ. Sci. Technol.*, 51, 6936-6944, 10.1021/acs.est.7b01210, 2017.
- 446 Huang, R.-J., Yang, L., Cao, J., Chen, Y., Chen, Q., Li, Y., Duan, J., Zhu, C., Dai, W., Wang, K., Lin, C., Ni, H.,
447 Corbin, J. C., Wu, Y., Zhang, R., Tie, X., Hoffmann, T., O'Dowd, C., and Dusek, U.: Brown Carbon Aerosol in
448 Urban Xi'an, Northwest China: The Composition and Light Absorption Properties, *Environ. Sci. Technol.*, 52,
449 6825-6833, 10.1021/acs.est.8b02386, 2018.
- 450 Jo, D. S., Park, R. J., Lee, S., Kim, S.-W., and Zhang, X.: A global simulation of brown carbon: implications for
451 photochemistry and direct radiative effect, *Atmos. Chem. Phys.*, 16, 3413-3432, 10.5194/acp-16-3413-2016,
452 2016.
- 453 Kampf, C. J., Jakob, R., and Hoffmann, T.: Identification and characterization of aging products in the
454 glyoxal/ammonium sulfate system - implications for light-absorbing material in atmospheric aerosols, *Atmos.
455 Chem. Phys.*, 12, 6323-6333, 10.5194/acp-12-6323-2012, 2012.
- 456 Laskin, A., Laskin, J., and Nizkorodov, S. A.: Chemistry of Atmospheric Brown Carbon, *Chem. Rev.*, 115, 4335-
457 4382, 10.1021/cr5006167, 2015.



- 458 Laskin, J., Laskin, A., Nizkorodov, S. A., Roach, P., Eckert, P., Gilles, M. K., Wang, B., Lee, H. J., and Hu, Q.:
459 Molecular Selectivity of Brown Carbon Chromophores, *Environ. Sci. Technol.*, 48, 12047-12055,
460 10.1021/es503432r, 2014.
- 461 Lee, H. J., Aiona, P. K., Laskin, A., Laskin, J., and Nizkorodov, S. A.: Effect of Solar Radiation on the Optical
462 Properties and Molecular Composition of Laboratory Proxies of Atmospheric Brown Carbon, *Environ. Sci.*
463 *Technol.*, 48, 10217-10226, 10.1021/es502515r, 2014.
- 464 Li, D., Wu, C., Zhang, S., Lei, Y., Lv, S., Du, W., Liu, S., Zhang, F., Liu, X., Liu, L., Meng, J., Wang, Y., Gao, J.,
465 and Wang, G.: Significant coal combustion contribution to water-soluble brown carbon during winter in Xingtai,
466 China: Optical properties and sources, *J. Environ. Sci.*, 124, 892-900, 10.1016/j.jes.2022.02.026, 2023.
- 467 Li, J., Zhang, Q., Wang, G., Li, J., Wu, C., Liu, L., Wang, J., Jiang, W., Li, L., Ho, K. F., and Cao, J.: Optical
468 properties and molecular compositions of water-soluble and water-insoluble brown carbon (BrC) aerosols in
469 northwest China, *Atmos. Chem. Phys.*, 20, 4889-4904, 10.5194/acp-20-4889-2020, 2020.
- 470 Li, L. J., Ho, S. S. H., Feng, B., Xu, H., Wang, T., Wu, R., Huang, W., Qu, L., Wang, Q., and Cao, J.: Characterization
471 of particulate-bound polycyclic aromatic compounds (PACs) and their oxidations in heavy polluted atmosphere:
472 A case study in urban Beijing, China during haze events, *Sci. Total Environ.*, 660, 1392-1402,
473 10.1016/j.scitotenv.2019.01.078, 2019a.
- 474 Li, X., Hu, M., Wang, Y., Xu, N., Fan, H., Zong, T., Wu, Z., Guo, S., Zhu, W., Chen, S., Dong, H., Zeng, L., Yu, X.,
475 and Tang, X.: Links between the optical properties and chemical compositions of brown carbon chromophores
476 in different environments: Contributions and formation of functionalized aromatic compounds, *Sci. Total*
477 *Environ.*, 786, 10.1016/j.scitotenv.2021.147418, 2021a.
- 478 Li, Y., Ji, Y., Zhao, J., Wang, Y., Shi, Q., Peng, J., Wang, Y., Wang, C., Zhang, F., Wang, Y., Seinfeld, J. H., and
479 Zhang, R.: Unexpected Oligomerization of Small alpha-Dicarbonyls for Secondary Organic Aerosol and Brown
480 Carbon Formation, *Environ. Sci. Technol.*, 55, 4430-4439, 10.1021/acs.est.0c08066, 2021b.
- 481 Li, Z., Nizkorodov, S. A., Chen, H., Lu, X., Yang, X., and Chen, J.: Nitrogen-containing secondary organic aerosol
482 formation by acrolein reaction with ammonia/ammonium, *Atmos. Chem. Phys.*, 19, 1343-1356, 10.5194/acp-
483 19-1343-2019, 2019b.
- 484 Lin, G., Penner, J. E., Flanner, M. G., Sillman, S., Xu, L., and Zhou, C.: Radiative forcing of organic aerosol in the
485 atmosphere and on snow: Effects of SOA and brown carbon, *J. Geophys. Res.-Atmos.*, 119, 7453-7476,
486 10.1002/2013jd021186, 2014.
- 487 Lin, P., Liu, J., Shilling, J. E., Kathmann, S. M., Laskin, J., and Laskin, A.: Molecular characterization of brown
488 carbon (BrC) chromophores in secondary organic aerosol generated from photo-oxidation of toluene, *Physical*
489 *Chemistry Chemical Physics*, 17, 23312-23325, 10.1039/c5cp02563j, 2015.
- 490 Liu, D., He, C., Schwarz, J. P., and Wang, X.: Lifecycle of light-absorbing carbonaceous aerosols in the atmosphere,
491 *npj Clim. Atmos. Sci.*, 3, 40, 10.1038/s41612-020-00145-8, 2020a.
- 492 Liu, S., Huang, D., Wang, Y., Zhang, S., Liu, X., Wu, C., Du, W., and Wang, G.: Synergetic effects of NH₃ and NO_x
493 on the production and optical absorption of secondary organic aerosol formation from toluene photooxidation,
494 *Atmos. Chem. Phys.*, 21, 17759-17773, 10.5194/acp-21-17759-2021, 2021.
- 495 Liu, S., Aiken, A. C., Gorkowski, K., Dubey, M. K., Cappa, C. D., Williams, L. R., Herndon, S. C., Massoli, P.,
496 Fortner, E. C., Chhabra, P. S., Brooks, W. A., Onasch, T. B., Jayne, J. T., Worsnop, D. R., China, S., Sharma,
497 N., Mazzoleni, C., Xu, L., Ng, N. L., Liu, D., Allan, J. D., Lee, J. D., Fleming, Z. L., Mohr, C., Zotter, P., Szidat,
498 S., and Prevot, A. S. H.: Enhanced light absorption by mixed source black and brown carbon particles in UK
499 winter, *Nature Communications*, 6, 10.1038/ncomms9435, 2015.
- 500 Liu, X., Wang, H., Wang, F., Lv, S., Wu, C., Zhao, Y., Zhang, S., Liu, S., Xu, X., Lei, Y., and Wang, G.: Secondary
501 Formation of Atmospheric Brown Carbon in China Haze: Implication for an Enhancing Role of Ammonia,



- 502 Environ. Sci. Technol., 57, 11163-11172, 10.1021/acs.est.3c03948, 2023a.
- 503 Liu, X. D., Wang, H. Y., Wang, F. L., Lv, S. J., Wu, C., Zhao, Y., Zhang, S., Liu, S. J., Xu, X. B., Lei, Y. L., and
504 Wang, G. H.: Secondary Formation of Atmospheric Brown Carbon in China Haze: Implication for an
505 Enhancing Role of Ammonia, Environmental Science & Technology, 57, 11163-11172,
506 10.1021/acs.est.3c03948, 2023b.
- 507 Liu, Y., Wang, T., Fang, X., Deng, Y., Cheng, H., Bacha, A.-U.-R., Nabi, I., and Zhang, L.: Brown carbon: An
508 underlying driving force for rapid atmospheric sulfate formation and haze event, Sci. Total Environ., 734,
509 139415, 10.1016/j.scitotenv.2020.139415, 2020b.
- 510 Lu, J. W., Flores, J. M., Lavi, A., Abo-Riziq, A., and Rudich, Y.: Changes in the optical properties of benzo a pyrene-
511 coated aerosols upon heterogeneous reactions with NO₂ and NO₃, Physical Chemistry Chemical Physics, 13,
512 6484-6492, 10.1039/c0cp02114h, 2011.
- 513 Lv, S., Wu, C., Wang, F., Liu, X., Zhang, S., Chen, Y., Zhang, F., Yang, Y., Wang, H., Huang, C., Fu, Q., Duan, Y.,
514 and Wang, G.: Nitrate-Enhanced Gas-to-Particle-Phase Partitioning of Water- Soluble Organic Compounds in
515 Chinese Urban Atmosphere: Implications for Secondary Organic Aerosol Formation, Environmental Science
516 & Technology Letters, 10, 14-20, 10.1021/acs.estlett.2c00894, 2023.
- 517 Meng, J., Wang, G., Li, J., Cheng, C., Ren, Y., Huang, Y., Cheng, Y., Cao, J., and Zhang, T.: Seasonal characteristics
518 of oxalic acid and related SOA in the free troposphere of Mt. Hua, central China: Implications for sources and
519 formation mechanisms, Sci. Total Environ., 493, 1088-1097, 10.1016/j.scitotenv.2014.04.086, 2014.
- 520 Moise, T., Flores, J. M., and Rudich, Y.: Optical Properties of Secondary Organic Aerosols and Their Changes by
521 Chemical Processes, Chem. Rev., 115, 4400-4439, 10.1021/cr5005259, 2015.
- 522 Nazarenko, L., Rind, D., Tsigaridis, K., Del Genio, A. D., Kelley, M., and Tausnev, N.: Interactive nature of climate
523 change and aerosol forcing, J. Geophys. Res.-Atmos., 122, 3457-3480, 10.1002/2016jd025809, 2017.
- 524 Qi, W. N., Zhang, Y. F., Shen, M. X., Li, L., Dai, W. T., Chen, Y. K., Liu, Y. L., Guo, X., Cao, Y., Wang, X., Jiang,
525 Y. K., and Li, J. J.: Comparison of Gas-Particle Partitioning of Glyoxal and Methylglyoxal in the Summertime
526 Atmosphere at the Foot and Top of Mount Hua, Molecules, 28, 10.3390/molecules28135276, 2023.
- 527 Qian, Y., Yasunari, T. J., Doherty, S. J., Flanner, M. G., Lau, W. K. M., Ming, J., Wang, H., Wang, M., Warren, S.
528 G., and Zhang, R.: Light-absorbing Particles in Snow and Ice: Measurement and Modeling of Climatic and
529 Hydrological impact, Adv. Atmos. Sci., 32, 64-91, 10.1007/s00376-014-0010-0, 2015.
- 530 Saleh, R., Marks, M., Heo, J., Adams, P. J., Donahue, N. M., and Robinson, A. L.: Contribution of brown carbon
531 and lensing to the direct radiative effect of carbonaceous aerosols from biomass and biofuel burning emissions,
532 J. Geophys. Res.-Atmos., 120, 10285-10296, 10.1002/2015jd023697, 2015.
- 533 Schnitzler, E. G., Gerrebos, N. G. A., Carter, T. S., Huang, Y., Heald, C. L., Bertram, A. K., and Abbatt, J. P. D.:
534 Rate of atmospheric brown carbon whitening governed by environmental conditions, Proceedings of the
535 National Academy of Sciences of the United States of America, 119, 10.1073/pnas.2205610119, 2022.
- 536 Sumlin, B. J., Pandey, A., Walker, M. J., Pattison, R. S., Williams, B. J., and Chakrabarty, R. K.: Atmospheric
537 Photooxidation Diminishes Light Absorption by Primary Brown Carbon Aerosol from Biomass Burning,
538 Environmental Science & Technology Letters, 4, 540-545, 10.1021/acs.estlett.7b00393, 2017.
- 539 Sun, Y., Zhang, Q., Zheng, M., Ding, X., Edgerton, E. S., and Wang, X.: Characterization and Source Apportionment
540 of Water-Soluble Organic Matter in Atmospheric Fine Particles (PM_{2.5}) with High-Resolution Aerosol Mass
541 Spectrometry and GC-MS, Environ. Sci. Technol., 45, 4854-4861, 10.1021/es200162h, 2011.
- 542 Van Damme, M., Clarisse, L., Whitburn, S., Hadji-Lazaro, J., Hurtmans, D., Clerbaux, C., and Coheur, P.-F.:
543 Industrial and agricultural ammonia point sources exposed, Nat., 564, 99-103, 10.1038/s41586-018-0747-1,
544 2018.
- 545 Vu, T. V., Shi, Z., Cheng, J., Zhang, Q., He, K., Wang, S., and Harrison, R. M.: Assessing the impact of clean air



- 546 action on air quality trends in Beijing using a machine learning technique, *Atmos. Chem. Phys.*, 19, 11303-
547 11314, 10.5194/acp-19-11303-2019, 2019.
- 548 Wang, D., Shen, Z., Zhang, Q., Lei, Y., Zhang, T., Huang, S., Sun, J., Xu, H., and Cao, J.: Winter brown carbon over
549 six of China's megacities: light absorption, molecular characterization, and improved source apportionment
550 revealed by multilayer perceptron neural network, *Atmos. Chem. Phys.*, 22, 14893-14904, 10.5194/acp-22-
551 14893-2022, 2022a.
- 552 Wang, G., Li, J., Cheng, C., Hu, S., Xie, M., Gao, S., Zhou, B., Dai, W., Cao, J., and An, Z.: Observation of
553 atmospheric aerosols at Mt. Hua and Mt. Tai in central and east China during spring 2009-Part 1: EC, OC and
554 inorganic ions, *Atmos. Chem. Phys.*, 11, 4221-4235, 10.5194/acp-11-4221-2011, 2011.
- 555 Wang, G. H., Kawamura, K., Lee, S., Ho, K. F., and Cao, J. J.: Molecular, seasonal, and spatial distributions of
556 organic aerosols from fourteen Chinese cities, *Environmental Science & Technology*, 40, 4619-4625,
557 10.1021/es060291x, 2006.
- 558 Wang, G. H., Zhang, R. Y., Gomez, M. E., Yang, L. X., Zamora, M. L., Hu, M., Lin, Y., Peng, J. F., Guo, S., Meng,
559 J. J., Li, J. J., Cheng, C. L., Hu, T. F., Ren, Y. Q., Wang, Y. S., Gao, J., Cao, J. J., An, Z. S., Zhou, W. J., Li, G.
560 H., Wang, J. Y., Tian, P. F., Marrero-Ortiz, W., Secrest, J., Du, Z. F., Zheng, J., Shang, D. J., Zeng, L. M., Shao,
561 M., Wang, W. G., Huang, Y., Wang, Y., Zhu, Y. J., Li, Y. X., Hu, J. X., Pan, B., Cai, L., Cheng, Y. T., Ji, Y. M.,
562 Zhang, F., Rosenfeld, D., Liss, P. S., Duce, R. A., Kolb, C. E., and Molina, M. J.: Persistent sulfate formation
563 from London Fog to Chinese haze, *Proceedings of the National Academy of Sciences of the United States of*
564 *America*, 113, 13630-13635, 10.1073/pnas.1616540113, 2016.
- 565 Wang, Q., Zhou, Y., Ma, N., Zhu, Y., Zhao, X., Zhu, S., Tao, J., Hong, J., Wu, W., Cheng, Y., and Su, H.: Review of
566 Brown Carbon Aerosols in China: Pollution Level, Optical Properties, and Emissions, *J. Geophys. Res.-Atmos.*,
567 127, 10.1029/2021jd035473, 2022b.
- 568 Wang, S. and Li, H.: NO₃ center dot-Initiated Gas-Phase Formation of Nitrated Phenolic Compounds in Polluted
569 Atmosphere, *Environ. Sci. Technol.*, 55, 2899-2907, 10.1021/acs.est.0c08041, 2021.
- 570 Wu, C., Cao, C., Li, J., Lv, S., Li, J., Liu, X., Zhang, S., Liu, S., Zhang, F., Meng, J., and Wang, G.: Different
571 physicochemical behaviors of nitrate and ammonium during transport: a case study on Mt. Hua, China, *Atmos.*
572 *Chem. Phys.*, 22, 15621-15635, 10.5194/acp-22-15621-2022, 2022.
- 573 Wu, C., Wang, G., Li, J., Li, J., Cao, C., Ge, S., Xie, Y., Chen, J., Li, X., Xue, G., Wang, X., Zhao, Z., and Cao, F.:
574 The characteristics of atmospheric brown carbon in Xi'an, inland China: sources, size distributions and optical
575 properties, *Atmos. Chem. Phys.*, 20, 2017-2030, 10.5194/acp-20-2017-2020, 2020.
- 576 Wu, C., Observation of Brown carbon and its optical properties on Mt. Hua, Zenodo [data set],
577 <https://doi.org/10.5281/zenodo.10926470>, 2024.
- 578 Wu, C., Synchronous observation of aerosol at Mt. Hua, Version 1, Zenodo [data set],
579 <https://doi.org/10.5281/zenodo.7413640>, 2022a.
- 580 Yan, C., Zheng, M., Bosch, C., Andersson, A., Desyaterik, Y., Sullivan, A. P., Collett, J. L., Zhao, B., Wang, S., He,
581 K., and Gustafsson, O.: Important fossil source contribution to brown carbon in Beijing during winter, *Sci. Rep.*,
582 7, 10.1038/srep43182, 2017.
- 583 Yan, J., Wang, X., Gong, P., Wang, C., and Cong, Z.: Review of brown carbon aerosols: Recent progress and
584 perspectives, *Sci. Total Environ.*, 634, 1475-1485, 10.1016/j.scitotenv.2018.04.083, 2018.
- 585 Yang, X., Ji, D., Li, J., He, J., Gong, C., Xu, X., Wang, Z., Liu, Y., Bi, F., Zhang, Z., and Chen, Y.: Impacts of
586 springtime biomass burning in Southeast Asia on atmospheric carbonaceous components over the Beibu Gulf
587 in China: Insights from aircraft observations, *Sci. Total Environ.*, 857, 10.1016/j.scitotenv.2022.159232, 2023.
- 588 Zhang, Y., Forrister, H., Liu, J., Dibb, J., Anderson, B., Schwarz, J. P., Perring, A. E., Jimenez, J. L., Campuzano-
589 Jost, P., Wang, Y., Nenes, A., and Weber, R. J.: Top-of-atmosphere radiative forcing affected by brown carbon



590 in the upper troposphere, *Nat. Geosci.*, 10, 486-489, 10.1038/ngeo2960, 2017.
591 Zhao, R., Lee, A. K. Y., Huang, L., Li, X., Yang, F., and Abbatt, J. P. D.: Photochemical processing of aqueous
592 atmospheric brown carbon, *Atmos. Chem. Phys.*, 15, 6087-6100, 10.5194/acp-15-6087-2015, 2015.



593
594
595
596
597
598
599
600
601

Table 1 Optical properties of BrC and mass concentrations organic carbon/nitrogen in PM_{2.5} and meteorological parameters at the two sampling sites.

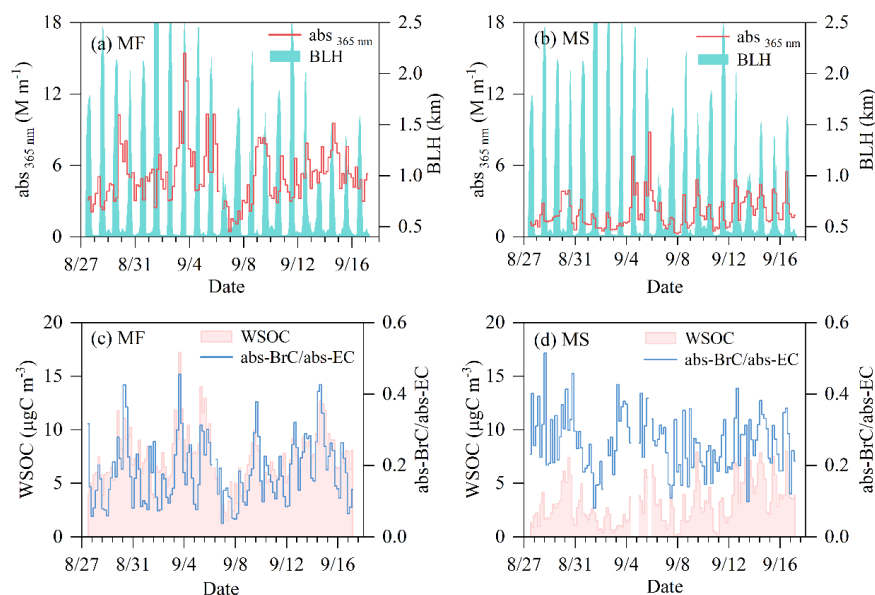
	Mountain foot (MF)			Mountainside (MS)		
	Average	Daytime	Nighttime	Average	Daytime	Nighttime
(i) Optical properties of BrC and acidity of PM_{2.5}						
abs ₃₆₅ (M m ⁻¹)	5.1±2.4	5.0±2.5	5.2±2.2	2.1±1.4	2.6±1.3	1.6±1.3
MAE ₃₆₅ (m ² g ⁻¹)	0.69±0.2	0.66±0.18	0.73±0.18	0.67±0.21	0.67±0.15	0.68±0.26
AAE	6.0±0.5	6.1±0.51	6.0±0.51	5.7±1.3	5.5±0.9	5.8±1.7
abs ₃₆₅ -BrC/abs ₅₅₀ -BC ^a	0.18±0.09	0.22±0.08	0.17±0.09	0.26±0.08	0.28±0.08	0.25±0.07
pH	2.9±2.0	2.3±1.6	3.6±2.1	3.4±2.2	3.5±2.2	3.3±2.2
(ii) Concentrations of carbonaceous PM_{2.5} and aerosol liquid water content (ALWC)						
WSOC (µgC m ⁻³)	7.3±2.5	7.6±2.8	7.0±2.1	3.2±2.1	4.0±2.1	2.4±1.7
WSON (µgN m ⁻³)	2.3±1.6	2.5±1.7	2.0±1.4	1.2±0.9	1.5±1.1	0.8±0.7
OC (µg m ⁻³)	14.0±4.7	12.4±4.6	15.4±4.4	5.0±2.8	6.3±2.8	3.8±2.3
EC (µg m ⁻³)	4.3±2.0	3.1±1.0	5.4±1.9	1.1±0.7	1.3±0.7	0.8±0.4
Nitrophenols (ng m ⁻³)	16±13	12±10	19±15	2.5±1.9	3.2±2.2	1.7±1.1
ALWC (µg m ⁻³)	28±64	11±15	44±86	27±71	18±24	35±95
WSOC/OC	0.54±0.15	0.62±0.13	0.47±0.11	0.62±0.21	0.62±0.16	0.61±0.25
(iii) Meteorological parameters						
T (°C)	23±4.2	27±3.0	20±2.4	15±2.5	16±2.3	14±2.3
RH (%)	69±18	56±14	81±14	63±20	62±19	63±21
Wind speed (m s ⁻¹)	1.3±1.1	1.5±0.93	1.2±1.2	3.2±2.0	2.7±1.5	3.8±2.3
Visibility (km)	14±9.5	16±9.6	12±9.0	22±12.1	21±12	24±12.0

602 ^aThe abs₅₅₀-BC was calculated according to the mass absorption efficiency (MAE) of BC (black
603 carbon) reported by Bosch et al. (2014), and the light wavelengths for the abs₃₆₅-BrC and abs₅₅₀-
604 BC are 365 nm and 550 nm, respectively.
605



606

607



608

609 **Figure 1. Temporal variations of light absorption of BrC in the ground surface (mountain**
610 **foot site, MF) and the upper boundary layer (mountainside site, MS) atmospheres in**
611 **inland China. (a, b) Abs_{365} and boundary layer height (BLH). (c, d) Concentration of WSOC**
612 **and the ratio of light absorption of BrC at $\lambda=365$ nm to BC at $\lambda= 550$ nm.**

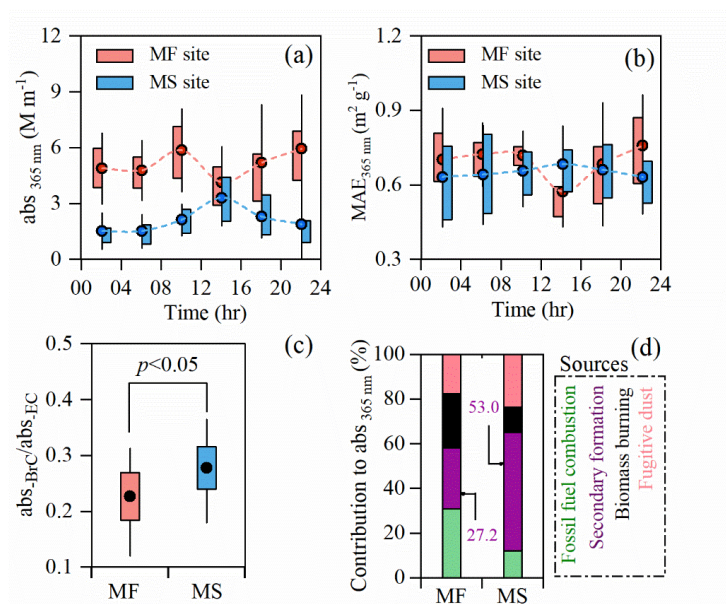
613

614



615

616

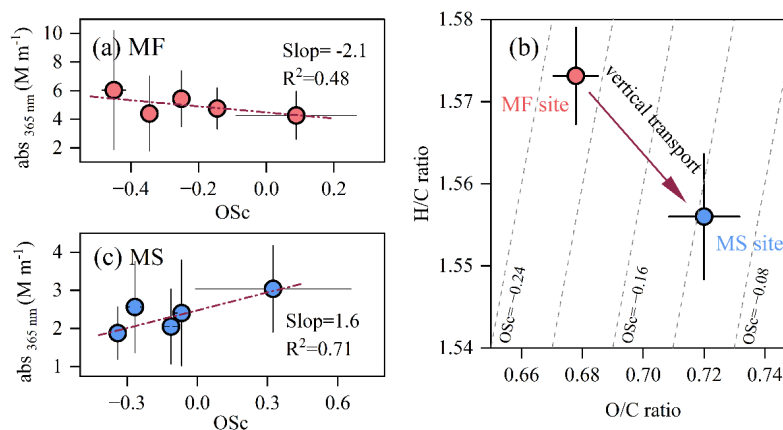


617

618 **Figure 2. BrC formation in air mass lifting process.** (a) and (b) Diurnal variations in $abs_{365\text{nm}}$
 619 and MAE at the mountain foot (MF) and mountainside (MS) sites. (c) Ratio of light absorption
 620 of BrC at $\lambda=365\text{ nm}$ to that of BC (abs_{BrC}/abs_{BC}) at $\lambda=550\text{ nm}$ in daytime at both sites (The
 621 abs_{BC} at $\lambda=550\text{ nm}$ was calculated according to mass absorption efficiency of EC reported by
 622 Bosch et al. (2014). (d) Source apportionment for the daytime BrC at the two sites.

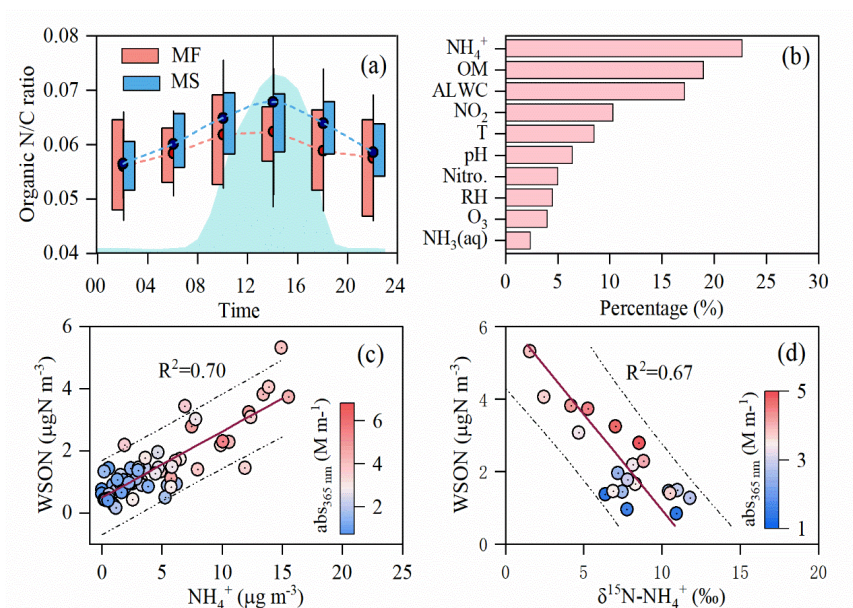


623
624
625
626
627
628



629
630
631
632
633
634
635
636
637
638
639
640
641
642

Figure 3. Evolution in chemical composition of daytime water-soluble BrC in the air mass transport from the mountain foot (MF site, red dots) to the mountainside (MS site, blue dots). (a) and (c) Light absorption (abs_{365}) of daytime water-soluble BrC as a function of their oxidation state ($\text{OSc} = 2\text{O}/\text{C} - \text{H}/\text{C}$) at MF and MS sites, respectively. (b) The VK-triangle diagram of water-soluble BrC at the two sites.



643

644 **Figure 4. Formation of water-soluble organic nitrogen compounds (WSONs) in the air**
 645 **mass lifting process.** (a) Diurnal variations in elemental ratio of N/C of fine particulate water-
 646 soluble organics at the mountain foot (MF) and mountainside (MS) sites. (b) Random forest
 647 analysis for the key factors affecting the WSON formation in the daytime PM_{2.5} at MS site. (c)
 648 and (d) Linear fit regressions for WSONs with NH₄⁺ and δ¹⁵N-NH₄⁺ in the daytime PM_{2.5}
 649 aerosols at MS site, respectively.

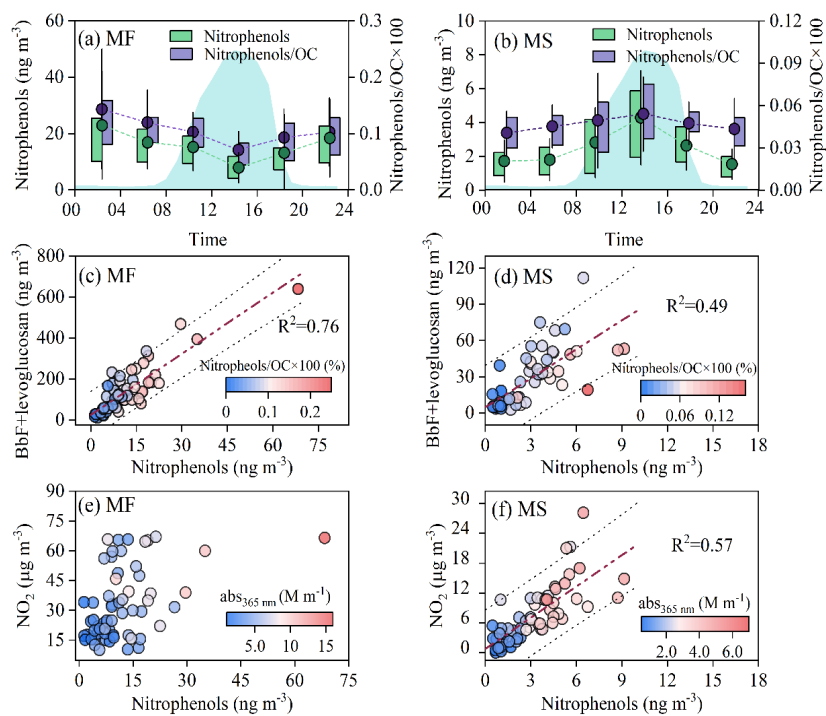
650

651



652

653



654

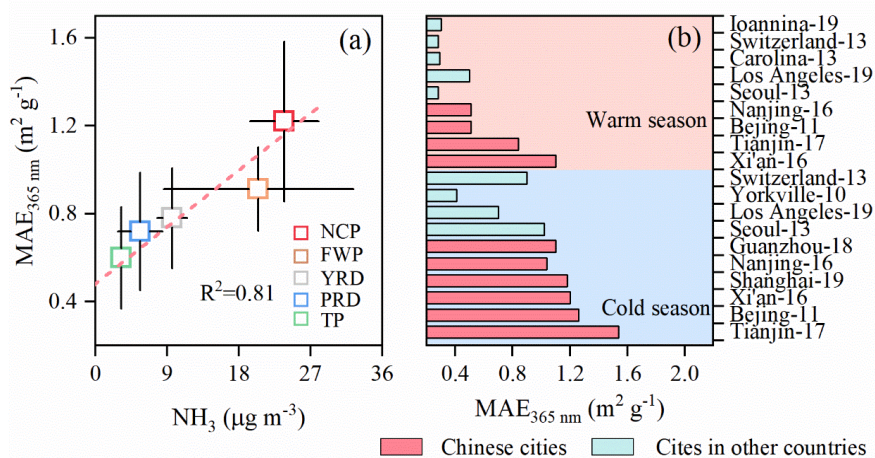
655 **Figure 5.** The source and secondary formation for nitrophenols at MF and MS sites. (a and b)

656 Diurnal variations in nitrophenols and mass ratio of nitrophenols to OC (nitrophenols/OC).

657 Linear fit regression for nitrophenols with BbF+levoglucosan (c and d) and NO₂ (e and f),

658 respectively.

659



660

661

662

663

664

665

666

Figure 6. Impact of NH_3 on atmospheric BrC over China. (a) Linear correlation between NH_3 and MAE of BrC in different regions of China (NCP, north China Plain; FWP: Fenwei Plain; YRD, Yangtze River delta; PRD, Pearl River delta; TP: Tibetan Plain). (b) $\text{MAE}_{365 \text{ nm}}$ of BrC in China and other countries (The details of datasets from literatures, including specific sites, time periods, and sources, etc., are given in Table S3 and S4).